

Lateral organic bilayer heterojunction photoconductors

John C. Ho,^{a)} Alexi Arango, and Vladimir Bulović^{b)}

Department of Electrical Engineering and Computer Science, Massachusetts Institute of Technology, Cambridge, Massachusetts 02139, USA

(Received 7 April 2008; accepted 30 May 2008; published online 14 August 2008)

We demonstrate a two-terminal, lateral organic bilayer photoconductor that generates an external quantum efficiency of $(12 \pm 1)\%$, with an internal quantum efficiency of $(140 \pm 2)\%$ indicative of photon-to-electron conversion gain. The photoconductor incorporates a heterojunction between *N,N'*-bis(3-methylphenyl)-*N,N'*-diphenyl-1,1'-biphenyl-4,4'-diamine (TPD) and 3,4,9,10-perylenetetracarboxylic bisbenzimidazole (PTCBI). Excitons generated with photoexcitation of PTCBI dissociate at the PTCBI/TPD interface and raise the charge carrier concentration in TPD, increasing device conductance. The exposed top surface enables interaction with chemical analytes in the environment, motivating the use of the photoconductor as a chemical sensor that transduces chemical signals into amplified changes in the electrical response. © 2008 American Institute of Physics. [DOI: 10.1063/1.2949317]

The strong optical response of organic thin films across the visible spectrum initially led to their use in the development of organic photoreceptor drums for xerography,¹ and more recently to demonstrations of thin film photodetectors² and solar cells.³ In a typical organic photodetector, photoactive organic thin films absorb the incident light to form excitons (bound electron-hole pairs) that can dissociate into charge carriers that are extracted by applying an external electric field. The vertical photodetector device geometries task the photoactive films with the dual role of exciton photogeneration and charge transport. The coupling of these two dissimilar roles in a single organic film constrains the design of photodetectors, requiring use of highly absorptive photoactive films that can simultaneously efficiently transport the photogenerated charge to the electrodes. Typically, amorphous organic thin films, while having desirable optical absorption characteristics, have low charge carrier mobilities due to the weak electrostatic interactions between van der Waals bonded molecules.⁴ Observing that the coupled functionality is due to the device architecture, in this letter we introduce a lateral heterojunction device geometry to help separate the exciton generation and charge transport, enabling independent optimization of the two processes in an amplifying photodetector structure.

We fabricate a two-terminal, lateral photoconductor that incorporates a heterojunction between an optically absorptive thin film that is primarily responsible for exciton generation, and another film that is optically transparent at the operating wavelength and is primarily responsible for charge transport.

The bilayer structure consists of two semiconducting thin films deposited over interdigitated gold electrodes [Fig. 1(a)]. Figure 1(b) shows the proposed energy band diagram indicating the highest occupied molecular orbital (HOMO) and the lowest unoccupied molecular orbital (LUMO) for the two semiconducting organic layers, while Fig. 1(c) depicts the cross section of the proposed device stack. Under steady state bias conditions, conduction can occur through either the

charge transport layer (CTL) or the exciton generation layer (EGL). With the proper choice of materials, conduction can predominantly occur in the CTL. Under illumination, light with an appropriate emission spectrum will be absorbed by the EGL, resulting in the formation of EGL excitons. A fraction $\eta_{\text{diffusion}}$ of the photogenerated excitons will diffuse to the EGL/CTL interface. If the EGL and CTL are aligned such that their offsets in either the LUMOs or HOMOs are greater than the binding energy of EGL excitons,⁵ as shown in Fig. 1(b), then it is energetically favorable for excitons to dissociate at the interface (dissociation efficiency η_D). Exciton dissociation in disordered organic materials has been attributed to both surface and bulk effects,⁴ with appropriately designed heterojunction interfaces achieving $\eta_D \sim 1$. Once created, the photogenerated charge will continue to accumulate at the EGL/CTL interface until equilibrium is achieved between carrier generation, bimolecular charge recombination at the interface, and charge diffusion away from the interface. In our structures, the accumulated, interfacial holes in the CTL will balance the electron charge accumulated in the EGL. The conductivity of the CTL is enhanced by the population of photogenerated charge carriers, which we mea-

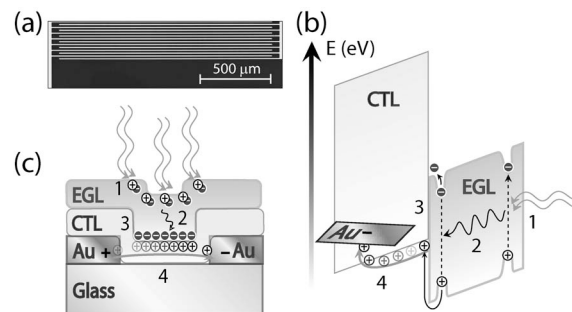


FIG. 1. The interdigitated gold fingers form 100 photoconductive channels each $1500 \pm 1 \mu\text{m}$ long and $10 \pm 1 \mu\text{m}$ wide yielding an effective device area of $1.5 \pm 0.15 \text{ mm}^2$. (a) An optical microscope image of device electrodes. (b) Energy band diagram of a lateral bilayer heterojunction photoconductor. (c) A cross-sectional view of the same bilayer device. Both illustrations depict the physical processes involved in steady-state device operation: (1) light absorption in EGL, (2) exciton diffusion through EGL, (3) exciton dissociation at EGL/CTL interface and charge transfer to CTL, and (4) charge transport.

^{a)}Electronic mail: ho_2002@mit.edu.

^{b)}Electronic mail: bulovic@mit.edu.

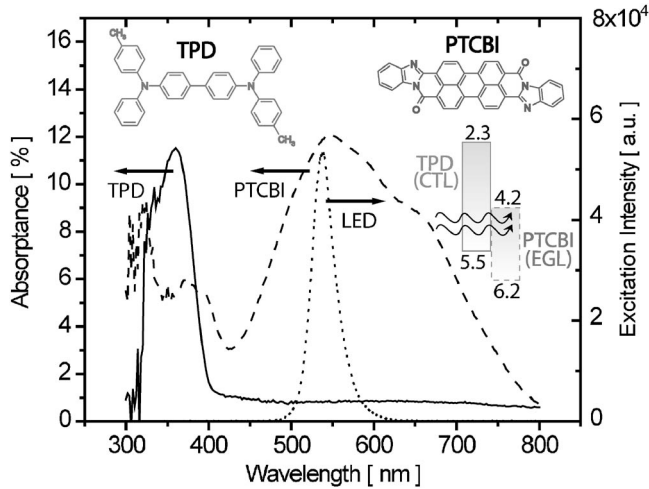


FIG. 2. Absorption spectra, chemical structure, and proposed energy band levels of the materials used in the bilayer heterojunction photoconductor: TPD as CTL and PTCBI as EGL. Also shown is the emission profile of the green LED (dotted line; $\lambda_{\text{peak}}=532$ nm) operated at an intensity of 40 mW/cm^2 . Energy band levels represent experimental values for the HOMO/LUMO based on photoemission spectroscopy data (Ref. 13).

sure as an increase in photocurrent through an illuminated, biased device.

To test this device model we use two molecular organic materials: *N,N'*-bis(3-methylphenyl)-*N,N'*-diphenyl-1,1'-biphenyl-4,4'-diamine (TPD) as CTL and 3,4,9,10-perylenetetracarboxylic bisbenzimidazole (PTCBI) as EGL, whose absorption spectra and electron energy band levels are depicted in Fig. 2. TPD (obtained from H.W. Sands) is a common hole transport material used in organic light emitting diodes (LEDs) and is optically transparent for wavelengths of $\lambda > 400$ nm, identifying it as suitable for use as the CTL. PTCBI (obtained from Sensient GmbH) is a perylene dye derivative that has found use as an optically absorptive material in organic solar cells⁶ with strong absorption across the visible spectrum, making it suitable for use as an EGL. From the absorption spectra in Fig. 2, we note that PTCBI can be optically excited independent of TPD by using a green LED centered at $\lambda=532$ nm (Lamina Light Engine, BL-3000). The thermally evaporated TPD/PTCBI films are deposited on a series of interdigitated gold electrodes that are photolithographically defined on glass [Fig. 1(a)]. These electrodes form a serpentine channel that is 150 ± 1 nm wide and $10 \pm 1 \mu\text{m}$ across, resulting in an effective device area of $1.5 \pm 0.15 \text{ mm}^2$.

Thin film absorption measurements are captured using a UV-vis-NIR spectrophotometer (NKD-8000, Aquila Instruments). The green LED light engine, powered by a sourcemeter (Keithley 2400), provides excitation with intensities of up to 40 mW/cm^2 as measured with a calibrated photodetector (Newport, 818-UV). The emission spectrum of the green LED was measured using a spectrometer (Ocean Optics, USB4000). Device current-voltage (*I-V*) characteristics were measured in a dark box using a picoammeter (Keithley 6487). Photocurrent spectra were measured using a digital lock-in amplifier (Stanford Research Systems, SR830) with monochromatic illumination provided by a 1000 W xenon arc lamp (Oriol) passed through a monochromator (Princeton Instruments/Acton Spectrapro 300i). The optical chopping frequency was set at 40 Hz, giving the device enough time to respond to the illumination. Both *I-V* characteristics and pho-

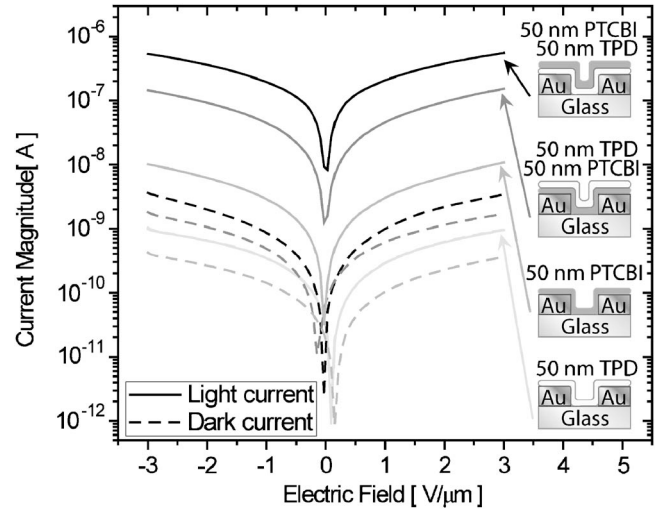


FIG. 3. Semilogarithmic plot of the current-voltage characteristics from a series of lateral photoconductor devices using TPD and PTCBI. Current-voltage sweeps are taken in the dark (dashed) and under illumination (solid) through the glass substrate from a 40 mW/cm^2 green LED ($\lambda_{\text{peak}} \sim 532$ nm). The inset cross-sectional diagrams describe the thicknesses and device structures. Both heterojunction devices [Au/PTCBI/TPD (black) and Au/TPD/PTCBI (dark gray)] exhibit steady-state photoresponse. The Au/TPD device (light gray) exhibits no photoresponse to the green LED, consistent with its absorption spectrum. The Au/PTCBI device (gray) exhibits a steady-state photoresponse with lower currents than heterojunction devices.

tocurrent spectra were taken in a nitrogen glovebox (MBraun) environment to prevent device degradation during measurements.

Figure 3 plots the steady state *I-V* characteristics, both with and without LED illumination, from a series of devices containing either single films or bilayer heterojunctions of PTCBI and TPD. The device that contains a single 50 ± 0.5 nm thick film of TPD generates no measurable photoresponse, which reflects the inability of TPD to absorb green ($\lambda=532$ nm) light. The thin film of PTCBI does generate a moderate photocurrent in response to the green light illumination, despite the absence of a heterojunction. The heterojunction devices show a comparative improvement in the photoresponse and a light to dark current ratio of over 100, which suggests that the TPD/PTCBI heterojunction interface is efficiently dissociating excitons.

Wavelength-resolved photocurrent spectra from three lateral photoconductors, containing films of PTCBI and TPD, are shown in Fig. 4. The photocurrent is measured with the lock-in amplifier locked to the light chopping frequency, effectively filtering out the dc dark current. TPD/PTCBI heterojunction devices are over 1000-fold higher as compared to external quantum efficiencies (EQEs), reaching an EQE of $(12 \pm 1)\%$ at $\lambda=552$ nm. Accounting for the number of photons absorbed in our thin films at that wavelength, the internal quantum efficiency for Au/TPD(5 ± 0.5 nm)/PTCBI(10 ± 0.5 nm) is $(140 \pm 2)\%$, when operated at an applied electric field of $1.25 \times 10^5 \text{ V/cm}$. An internal quantum efficiency of greater than 100% indicates an optical-to-electrical conversion gain in the device.

Under steady state conditions, the photocurrent gain represents the ratio of the photogenerated charge carrier lifetime to the transit time across the device of charge carriers injected at the contacts.⁷ In the steady state, the total carrier generation rate must be equal to the total carrier recombina-

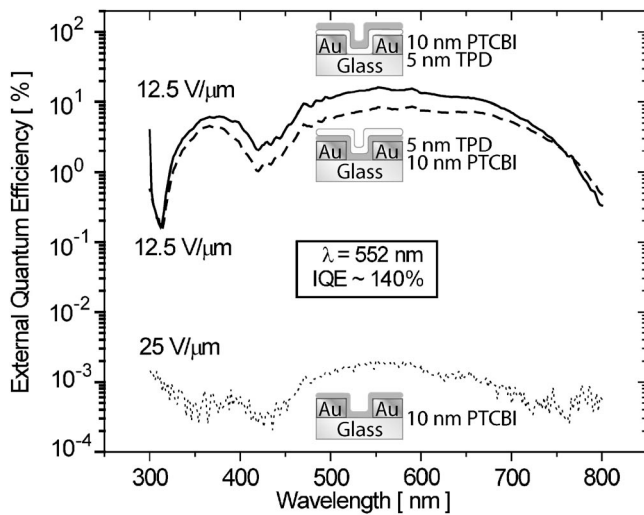


FIG. 4. Semilogarithmic plot of EQE vs wavelength, for the series of device structures illustrated. Electric fields applied during the measurement are indicated. The Au/TPD device yields no measurable photoresponse. Both heterojunction devices (solid and dashed lines) exhibit over 1000-fold improvement in the EQE over the Au/PTCBI device (dotted line), at twofold lower bias voltages. At $\lambda = 552$ nm, the Au/PTCBI/TPD device and Au/TPD/PTCBI device yield EQEs of $(8 \pm 1)\%$ and $(12 \pm 1)\%$ respectively. Accounting for the absorption of $\lambda = 552$ nm light in the PTCBI/TPD device, we find an internal quantum efficiency of $(140 \pm 2)\%$.

tion rate, which can be written as the following relation:

$$\frac{n}{\tau}d = \eta\Phi,$$

where n is the charge carrier number density, τ is the carrier lifetime, d is the device thickness, η is the photoluminescence efficiency of the active material, and Φ is the incident photon flux per unit area. Assuming uniform charge density in the lateral direction along current flow, device photocurrent can be modeled by the one dimensional drift current density with electron and hole densities equal ($n=p$). μ_n and μ_p are the electron and hole mobilities, respectively, and E is the applied electric field. Substituting the steady state condition relation and solving for the total current density yields

$$J_{\text{photo}} = qn(\mu_n + \mu_p)E = q\eta\Phi\frac{L}{d} \times \tau\left(\frac{1}{t_n} + \frac{1}{t_p}\right).$$

L is the device channel length and t_n and t_p are the electron and hole transit times, respectively. In amorphous organic thin films it has been shown that energetic and spatial disorder^{8,9} can lead to a significant population of energetic traps, which can be filled by the excess photogenerated carriers, yielding a higher effective mobility while the trapped charge persists in the nonequilibrium states. The time it takes for trapped charge to relax is dependent on the disorder in the film, so much so that the carrier transit time can be shorter than the carrier lifetime in strongly disordered materials. Thus, for every photoexcited carrier, many more carriers can be transported across the film before the photoexcited carriers relax, which leads to photoconductive gains above unity.

The structure of the lateral heterojunction photoconductor exposes the top surface of the EGL to the external envi-

ronment, necessitating device encapsulation with either an inert thin film of wide optical bandgap or packaging in an inert gas environment. Alternatively, leaving the top EGL surface unpackaged allows the bilayer photoconductor structure to be used as a chemiresistor that separates the chemosensing and conduction functions across the EGL and CTL, respectively, enabling independent optimization of the two device functions. By incorporating a chemosensitive fluorescent conjugated polymer^{10–12} as the EGL, we envision a vapor-phase, solid-state chemical sensor architecture that utilizes the sensing properties of the fluorescent polymer while maintaining the chemiresistor's simple transduction of chemical to electrical signals. When using a chemosensitive fluorescent polymer the exciton generation not only depends on the intensity of incident light excitation, but also on the presence of analytes in the local environment.¹¹ The photoluminescence efficiency η of chemosensitive fluorescent polymers is strongly modulated by a chemical signal. As the photoconductive gain is related to the incident light intensity, the sensor's sensitivity can be tuned by changing the incident light signal, giving the sensor a large dynamic range.

The lateral bilayer photoconductor structure presented here exhibits gain and is shown to generate photocurrent exclusively from absorption in the PTCBI film. In contrast to a single layer photoconductor, the bilayer device separates the charge generation mechanism from the charge transport mechanism. Doing so allows the engineering of each layer for optimized light to dark current ratio or adding chemical sensing abilities.

This work was supported by funding from the Institute for Soldier Nanotechnology (ISN) and was supported in part by the MRSEC Program of the National Science Foundation under Award No. DMR 02-13282. In addition this work made use of the Shared Experimental Facilities supported in part by the MRSEC Program of the National Science Foundation under Award No. DMR 02-13282. The authors would also like to thank Ivan Nausieda for his help in processing the photolithographically defined substrates.

¹P. M. Borsenberger and D. S. Weiss, *Organic Photoreceptors for Xerography* (Dekker, New York, 1998).

²B. P. Rand, J. Genoe, P. Heremans, and J. Poortmans, *Prog. Photovoltaics* **15**, 659 (2007).

³P. Peumans, A. Yakimov, and S. R. Forrest, *J. Appl. Phys.* **93**, 3693 (2003).

⁴M. Pope and C. E. Swenberg, *Electronic Processes in Organic Crystals and Polymers*, 2nd ed. (Oxford University Press, New York, 1999).

⁵B. P. Rand, D. P. Burk, and S. R. Forrest, *Phys. Rev. B* **75**, 115327 (2007).

⁶P. Peumans, S. Uchida, and S. R. Forrest, *Nature (London)* **425**, 158 (2003).

⁷S. M. Sze and K. K. Ng, *Physics of Semiconductor Devices*, 3rd ed. (Wiley, Hoboken, 2007).

⁸C. Madigan and V. Bulovic, *Phys. Rev. Lett.* **91**, 247403 (2003).

⁹C. Madigan and V. Bulovic, *Phys. Rev. Lett.* **96**, 046404 (2006).

¹⁰B. Lourdes, D. N. Reinhoudt, and M. Crego-Calama, *Chem. Soc. Rev.* **36**, 993 (2007).

¹¹S. W. Thomas, G. D. Joly, and T. M. Swager, *Chem. Rev. (Washington, D.C.)* **107**, 1339 (2007).

¹²A. Rose, Z. G. Zhu, C. F. Madigan, T. M. Swager, and V. Bulovic, *Nature (London)* **434**, 876 (2005).

¹³W. R. Salaneck, K. Seki, A. Kahn, and J. Pireaux, *Conjugated Polymer and Molecular Interfaces* (Dekker, New York, 2002).